Stem Cell Reports
Report

ISSCR

OPEN ACCESS

An Embryonic Stem Cell-Specific NuRD Complex Functions through Interaction with WDR5

Ly-Sha Ee,[1] Kurtis N. McCannell,[1] Yang Tang,[2] Nancy Fernandes,[2] W. Rod Hardy,[1] Michael R. Green,[1,3] Feixia Chu,[2] and Thomas G. Fazzio[1,*]

[1]Department of Molecular, Cell, and Cancer Biology, University of Massachusetts Medical School, Worcester, MA 01605, USA
[2]Department of Molecular, Cellular, and Biomedical Sciences, University of New Hampshire, Durham, NH 03824, USA
[3]Howard Hughes Medical Institute, University of Massachusetts Medical School, Worcester, MA 01605, USA
*Correspondence: thomas.fazzio@umassmed.edu
http://dx.doi.org/10.1016/j.stemcr.2017.04.020

SUMMARY

The Nucleosome Remodeling and Deacetylase (NuRD) complex is a chromatin regulatory complex that functions as a transcriptional co-repressor in metazoans. The NuRD subunit MBD3 is essential for targeting and assembly of a functional NuRD complex as well as embryonic stem cell (ESC) pluripotency. Three MBD3 isoforms (MBD3A, MBD3B, and MBD3C) are expressed in mouse. Here, we find that the MBD3C isoform contains a unique 50-amino-acid N-terminal region that is necessary for MBD3C to specifically interact with the histone H3 binding protein WDR5. Domain analyses of WDR5 reveal that the H3 binding pocket is required for interaction with MBD3C. We find that while *Mbd3c* knockout ESCs differentiate normally, MBD3C is redundant with the MBD3A and MBD3B isoforms in regulation of gene expression, with the unique MBD3C N terminus required for this redundancy. Together, our data characterize a unique NuRD complex variant that functions specifically in ESCs.

INTRODUCTION

To maintain their cellular identity, embryonic stem cells (ESCs) utilize a network of core transcription factors and chromatin remodeling enzymes that bind and regulate pluripotency genes and differentiation genes in response to developmental signaling (Kim et al., 2008). The Nucleosome Remodeling and Deacetylase (NuRD) complex is unique among chromatin regulators because it couples ATP-dependent nucleosome remodeling activity with histone modification (deacetylase) activity (Tong et al., 1998; Wade et al., 1998; Xue et al., 1998; Zhang et al., 1998). NuRD alters nucleosome occupancy to block the binding of transcriptional machinery at gene promoters, thus functioning primarily as a co-repressor (Denslow and Wade, 2007; Yildirim et al., 2011). In addition, mice deleted for the *Mbd3* gene, which encodes a NuRD subunit important for NuRD targeting and assembly, are nonviable (Hendrich et al., 2001). ESCs derived from *Mbd3*-null mouse embryos do not differentiate and are capable of self-renewal in culture in the absence of leukemia inhibitory factor (LIF) (Kaji et al., 2006). *Mbd3* was subsequently shown to be important for differentiation and development through silencing of pluripotency genes (Reynolds et al., 2012), functioning in part by deacetylation of H3K27 (Reynolds et al., 2011).

MBD3 was originally identified as a member of the methyl-CpG binding domain (MBD) family of proteins (Hendrich and Bird, 1998). However, unlike MBD members MECP2 and MBD1, 2, and 4, MBD3 does not bind methylated DNA (Hendrich and Bird, 1998; Zhang et al., 1999). Three MBD3 isoforms (MBD3A, B, and C) are expressed in mouse ESCs, and only MBD3A has a full-length MBD (Kaji et al., 2006). Thus, the possibility exists for formation of multiple NuRD complexes of varying subunit combinations and functional specificities.

Here, we have characterized a unique variant of the NuRD chromatin remodeling complex that harbors MBD3C, an ESC-specific isoform of MBD3, as well as the histone H3 binding protein WDR5. MBD3C is expressed almost exclusively in ESCs via an alternative CpG island (CGI)-containing promoter located in the second intron of the *Mbd3* gene. We further show that MBD3C contains a unique 50-amino-acid N terminus that is necessary for WDR5 interaction. MBD3C interacts with the WDR5 H3 binding pocket through an arginine-containing motif also utilized by MLL1 for WDR5 binding. RNA sequencing (RNA-seq) analysis revealed that the three MBD3 isoforms are largely redundant for gene regulation, since knockout (KO) of all three isoforms had a more severe effect on gene expression than individual KO of *Mbd3c* or simultaneous KO of *Mbd3a* and *Mbd3b*. Importantly, the WDR5-interaction domain of *Mbd3c* is critical for its gene regulatory function, suggesting that WDR5 plays critical roles in MBD3C/NuRD complex.

RESULTS AND DISCUSSION

MBD3C/NuRD Co-purifies with WDR5

To identify proteins co-purifying with MBD3 in ESCs, we used a cell line in which one copy of endogenous MBD3

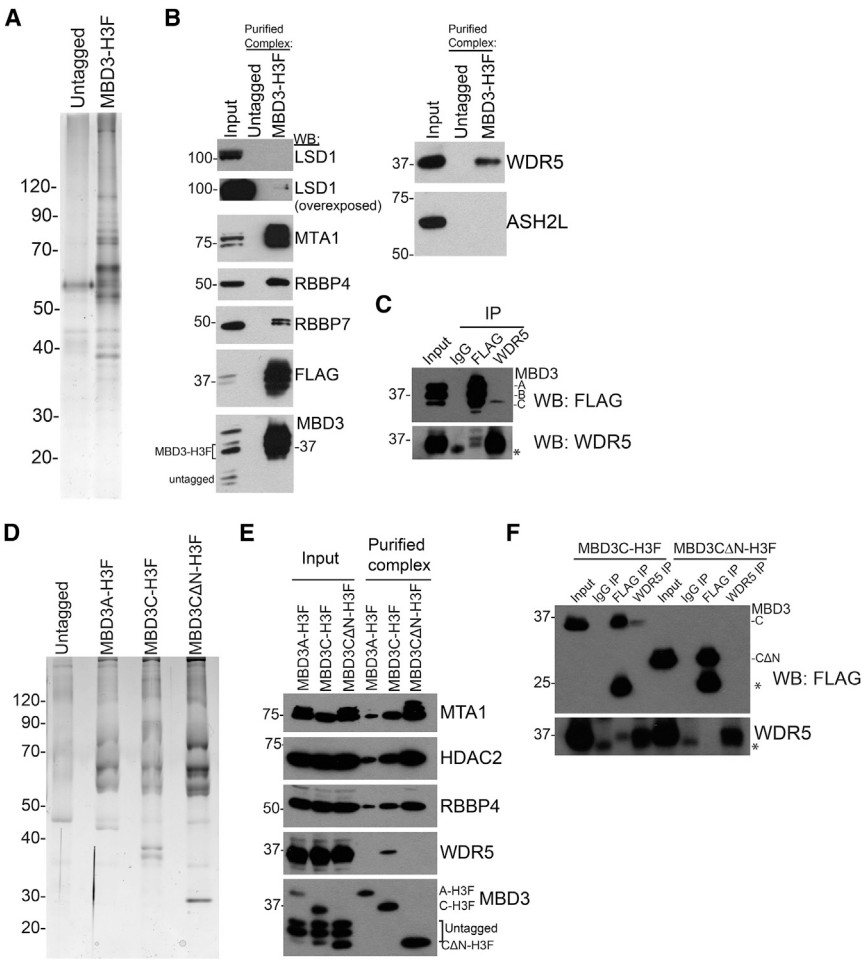

Figure 1. The NuRD Subunit MBD3C Co-purifies with WDR5

(A) Silver stain of MBD3-H3F complex.

(B) Western blot (WB) of purified complex from (A) showing interaction of MBD3 with NuRD subunits (left) and with WDR5 or MLL subunit ASH2L (right).

(C) Western blots for MBD3-H3F or WDR5 upon immunoprecipitation (IP) of each. Asterisk indicates immunoglobulin G (IgG).

(D) Silver stain of MBD3 complex expressing individually H3F-tagged MBD3 isoforms.

(E) Western blot of purified complexes from (D) showing interaction with WDR5 and NuRD subunits.

(F) WDR5 or FLAG immunoprecipitation from individually tagged MBD3C-H3F and MBD3CΔN-H3F ESCs. Asterisks indicate IgG.

is fused to a C-terminal 6xHis-3xFLAG tag (*Mbd3-H3F*; Yildirim et al., 2011), allowing for affinity purification of MBD3A, B, and C simultaneously (Figures 1A and S1A). Liquid chromatography-tandem mass spectrometry (LC-MS/MS) of purified MBD3 complexes identified all canonical NuRD subunits, several of which were subsequently confirmed by western blot (Figure 1B and Table S1).

Consistent with recent MS analyses of NuRD components (Bode et al., 2016), we detected an interaction between MBD3 and the SET/MLL complex component WDR5 (Figures 1B and S1B; Table S1). The MLL complex is a histone methyltransferase that catalyzes methylation of H3K4, a mark found at transcriptionally active genes (Bernstein et al., 2002; Santos-Rosa et al., 2002). WDR5 binds the histone H3 tail in vitro and is essential for H3K4 trimethylation and MLL complex formation (Couture et al., 2006; Dou et al., 2006; Ruthenburg et al., 2006; Schuetz et al., 2006; Wysocka et al., 2005). We did not observe any other MLL subunits co-purifying with MBD3 (Figure 1B and Table S1), suggesting that WDR5 interacts with MBD3/NuRD independently of MLL complex. To validate these data, we performed co-immunoprecipitation (coIP) assays. Interestingly, WDR5 immunoprecipitation pulled down MBD3C, but not the more abundant isoforms, MBD3A and B (Figure 1C). These data suggest that WDR5 interacts specifically with this smallest and least characterized isoform of MBD3.

To further investigate the composition of the MBD3C/NuRD complex, we generated an ESC line expressing *Mbd3c-H3F* from a viral vector, such that only the MBD3C isoform is epitope-tagged. To this end, we first performed 5′ rapid amplification of cDNA ends (5′-RACE) to obtain the *Mbd3c* coding sequence. We found that MBD3C is translated from a start codon within intron 2 of the *Mbd3* gene, consistent with a recent report (dos Santos et al., 2014). Thus, MBD3C lacks the entire MBD and contains a unique 50-amino-acid N terminus (Figure S1C). MBD3C-H3F complexes were affinity purified (Figure 1D) and analyzed by LC-MS/MS. As expected, WDR5 co-purifies with MBD3C-H3F but not MBD3A-H3F (Figures 1E and S1D; Table S2). Importantly, we found that WDR5 interaction was disrupted by deletion of the unique

MBD3C N terminus (MBD3CΔN; Figures 1E and S1D), demonstrating that this domain is necessary for WDR5 binding. CoIP experiments confirmed these results (Figure 1F). Furthermore, we observed that MBD3C-H3F, MBD3A-H3F, and MBD3CΔN-H3F all co-purify with the canonical NuRD subunits (Figures 1E and S1D; Table S2). Together with data showing that WDR5 also co-purifies with NuRD subunits (Figure S1B; Bode et al., 2016) and that MBD3C co-fractionates exclusively with NuRD subunit MTA1 (Figure S1E), these data demonstrate that MBD3C assembles into a canonical NuRD complex that also includes WDR5. Although the MBD3 MBD was previously shown to directly interact with NuRD subunits HDAC1 and MTA2 in vitro (Saito and Ishikawa, 2002), our findings suggest that HDAC1 and MTA2 can also associate with the NuRD complex by MBD-independent mechanisms in vivo. In addition, while the unique MBD3C N terminus is required for interaction with WDR5, it is dispensable for interaction with the other known NuRD subunits (Figure S1D and Table S2).

The WDR5 Histone H3 Binding Pocket Is Required for Interaction with MBD3C

To gain insight into the functions of the MBD3C-WDR5 interaction, we dissected the domains within MBD3C and WDR5 important for their interaction. WDR5 contains two binding surfaces on opposite sides of the protein, one that binds the histone H3 N-terminal tail or the SET/MLL complex subunit MLL1, and another that binds both the SET/MLL subunit RBBP5 (Figure 2A; Odho et al., 2010; Patel et al., 2008; Song and Kingston, 2008) and long noncoding RNAs (Yang et al., 2014). To test whether MBD3C interacts with either WDR5 binding surface, we performed coIPs in 293T cells co-transfected with vectors expressing MBD3C-H3F and FLAG-tagged point mutants from both binding surfaces of WDR5: D107A on the H3K4/MLL1 binding surface and F266A, K250A, and R181A on the RBBP5/RNA binding surface (Yang et al., 2014). We found that the F266A, K250A, and R181A mutants of WDR5 co-immunoprecipitate with antibodies recognizing endogenous MBD3 (Figure 2B). In contrast, the D107A mutant was absent from MBD3 immunoprecipitates, suggesting that MBD3C binds near or within the WDR5 H3K4/MLL1 binding pocket.

To extend these findings, we generated a series of truncation mutants of the 50-amino-acid MBD3C N terminus to pinpoint the residues necessary for binding (Figure 2C). Deletion of the first 40 amino acids of H3F-tagged MBD3C did not disrupt the interaction with V5-tagged WDR5 (Figure 2D). However, upon deletion of amino acids 41–50 of MBD3C, interaction with WDR5 was completely lost (Figure 2E), as we observed for MBD3C mutants lacking amino acids 1–50 (Figures 1E, 1F, and 2D). Furthermore, an N-terminal fusion of amino acids 41–50 to the MBD3A isoform was sufficient to allow MBD3A to bind WDR5 (Figure 2F). These data demonstrate that amino acids 41–50 of MBD3C mediate WDR5 binding (see also Figure S1B).

MLL1, KANSL1, and histone H3 all bind the same domain on WDR5 via a 2-amino-acid alanine-arginine (AR) motif present on each protein (Couture et al., 2006; Han et al., 2006; Patel et al., 2008; Ruthenburg et al., 2006; Schuetz et al., 2006; Song and Kingston, 2008; Dias et al., 2014; Figures 2A and 2G). MBD3C contains an AR dipeptide within its N-terminal WDR5 binding domain (A42-R43; Figure 2G), which we hypothesized to be necessary for WDR5 binding. Confirming our hypothesis, an R43A mutant of MBD3C failed to pull down WDR5 (Figure 2E). Together, these data indicate that MBD3C, histone H3, and MLL1 use a common motif to bind the same surface of WDR5. We observed slightly reduced MBD3C protein levels in cells expressing mutants of MBD3C or WDR5 that disrupt MBD3C-WDR5 binding (Figures 2D and 2E), raising the possibility that interaction with WDR5 plays a role in stabilizing MBD3C.

Mbd3c Expression Is Largely Restricted to Pluripotent Stem Cells

The *Mbd3c* isoform appears to be highly expressed only in ESCs, as it is absent or weakly expressed in mouse embryonic fibroblasts (MEFs) and all adult tissues tested (Figures S1A and S2A). To determine when *Mbd3c* expression is lost during differentiation, we subjected ESCs to a 10-day embryoid body (EB) differentiation time course. We observed that MBD3C protein was lost between days 4 and 6 of the time course with kinetics similar to loss of OCT4 protein during differentiation (Figure 3A).

Next, we tested whether *Mbd3c* expression was restored upon reprogramming of differentiated cells to induced pluripotent stem cells. Primary MEFs were infected with doxycycline (dox)-inducible lentiviruses expressing reprogramming factors OCT4, SOX2, and KLF4 marked with an mCherry reporter (OSK-mCherry), L-MYC, and a lentiviral EOS-EGFP reporter specifically activated in pluripotent cells (Hotta et al., 2009). Infected cells were cultured with dox for 20 days. After an additional 10 days in the absence of dox, cells were imaged and stained for alkaline phosphatase to verify silencing of OSK-mCherry and presence of ESC-like colonies (Figures S3A and S3B). Lysates for western blots were prepared from expanded induced pluripotent stem cell (iPSC) colonies picked at 30 days. We observed that reprogrammed iPSC colonies express *Mbd3c* (Figure 3B). These data demonstrate that *Mbd3c* expression is restored when somatic cells are reprogrammed to iPSCs.

Finally, to investigate how *Mbd3c* expression might be silenced during differentiation, we performed bisulfite

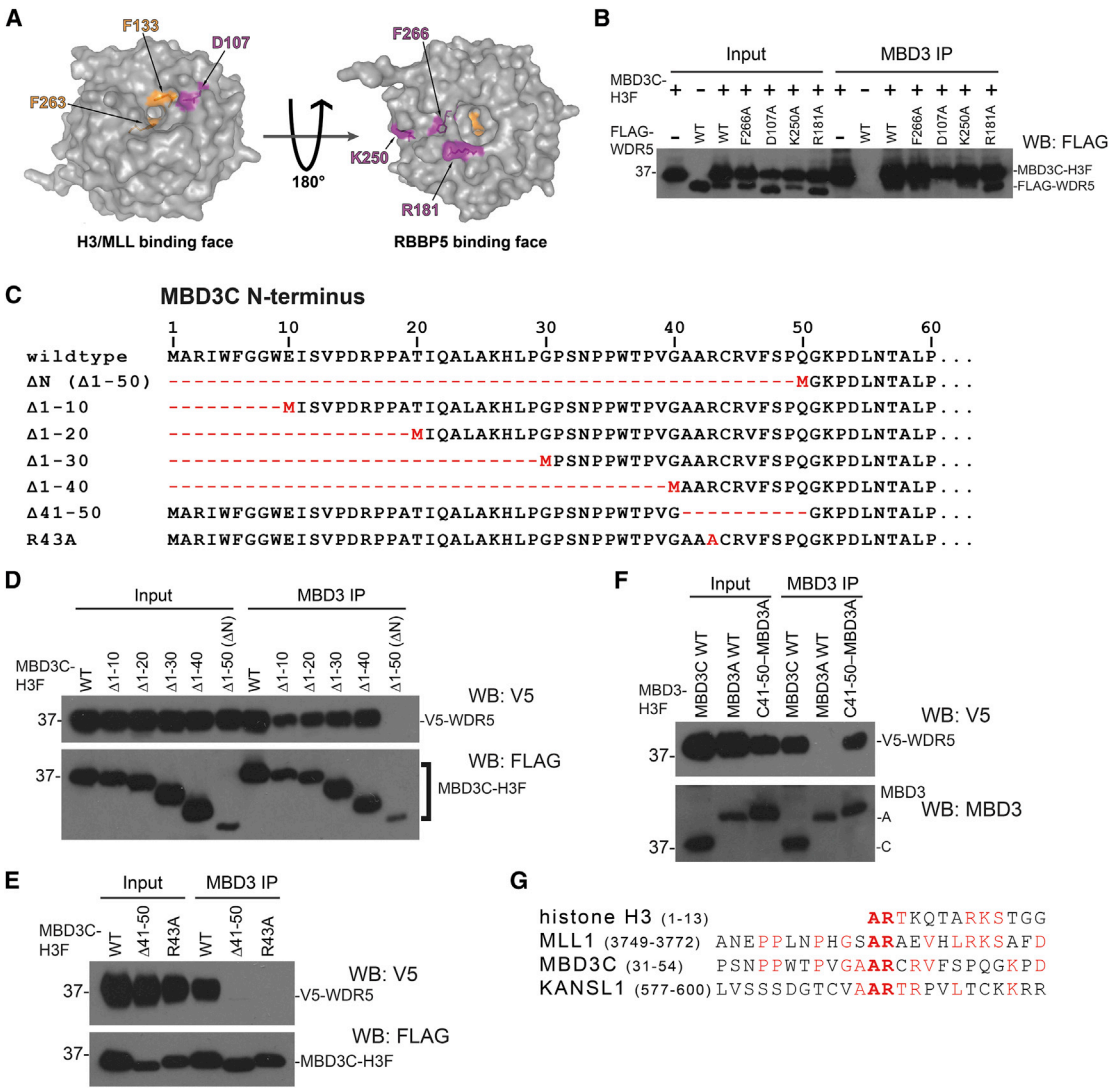

Figure 2. The WDR5 Histone H3 Binding Pocket Is Required to Bind MBD3C

(A) PyMol depiction of WDR5 crystal structure (PDB: 2GNQ) showing the H3K4/MLL1 (left) and RBBP5 (right) binding pockets. Residues individually mutated to alanine (Yang et al., 2014) are shown in magenta. Residues necessary for MLL1 R3761 or histone H3 R2 binding are shown in orange.

(B) CoIPs with MBD3 antibody from 293T cells co-transfected with expression vectors carrying MBD3C-H3F and indicated FLAG-tagged WDR5 mutants.

(C) Schematic of *Mbd3c* N-terminal mutant constructs used in (D) and (E).

(D–F) CoIPs with MBD3 antibody in 293T cells performed as in (B), using V5-tagged WDR5 constructs and H3F-tagged MBD3 constructs. For "C41-50—MBD3A," MBD3C amino acids 41–50 were fused to the N terminus of the MBD3A isoform.

(G) Alignment of the MBD3C N terminus with WDR5-binding regions of mouse MLL1, KANSL1, and histone H3.

pyrosequencing analysis on the *Mbd3c* promoter during an EB differentiation time course. The *Mbd3* gene contains a ~350-bp CGI which spans exon 2 and part of intron 2, and overlaps with the sequence encoding the MBD3C N-terminal domain (Figure 3C). We measured methylation of 11 individual CpGs within the *Mbd3c* promoter and observed a large increase in methylation at all sites over the differentiation time course (Figure 3D). Methylation increased most dramatically around day 4, which corresponds to the timing of MBD3C loss during differentiation (Figure 3A). Therefore, silencing of *Mbd3c* expression during differentiation is likely due to increased methylation of the *Mbd3c* promoter CGI.

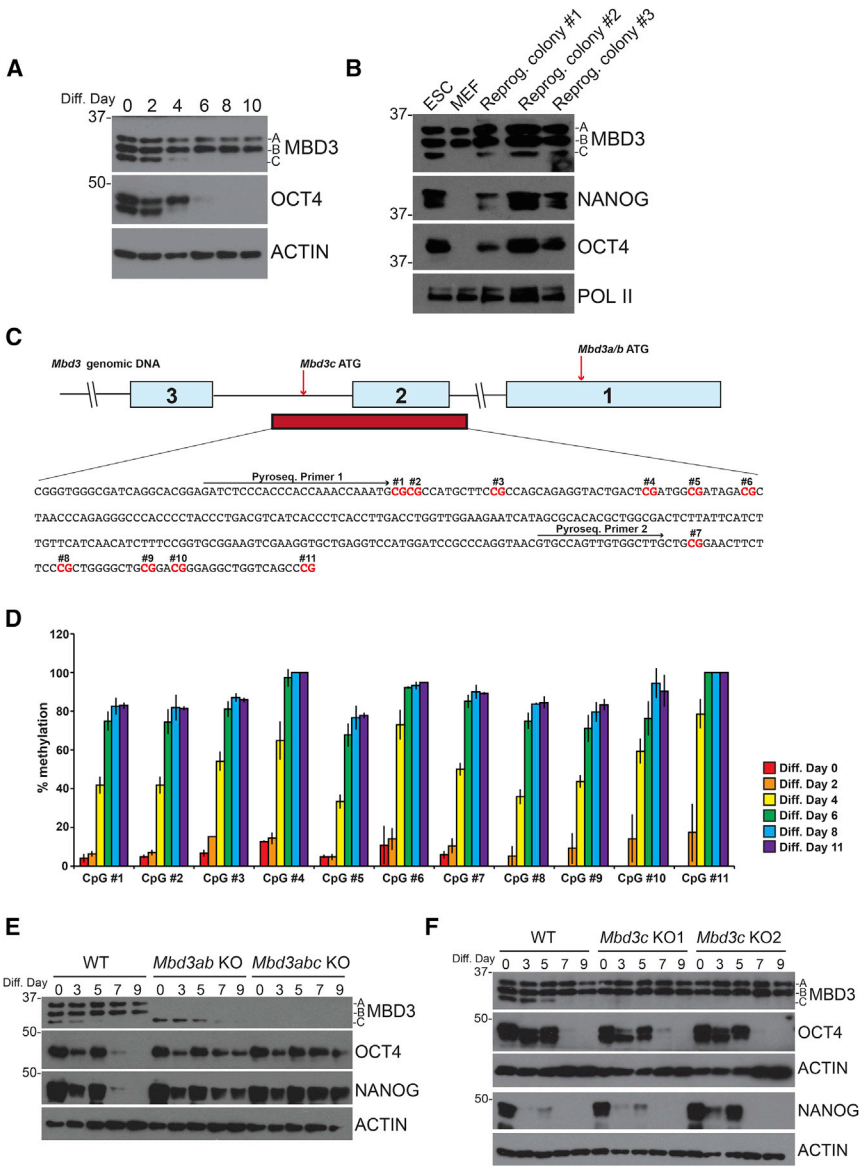

Figure 3. *Mbd3c* Is Dispensable for ESC Differentiation

(A) Western blots from ESCs differentiated over 10 days. Actin serves as a loading control.

(B) Western blots from primary MEFs reprogrammed to iPSCs.

(C) Schematic of the *Mbd3* gene showing the sequence and location of the *Mbd3c* promoter CpG island (red bar). Light-blue boxes indicate exons. CpGs tested for methylation are highlighted in red.

(D) Pyrosequencing of bisulfite-converted DNA from cells collected at the indicated differentiation time points. Error bars represent the SD of three biological replicates.

(E and F) Western blots of differentiating *Mbd3ab* and *Mbd3abc* KO cells (E) and two clonal *Mbd3c* KO lines (F). WT, wild-type.

Mbd3c Is Dispensable for ESC Differentiation

Mbd3-null ESCs exhibit pluripotency defects and are capable of self-renewal in the absence of LIF (Kaji et al., 2006). We therefore wanted to test whether the MBD3C isoform was specifically required for early stages of differentiation. We generated homozygous *Mbd3c*, *Mbd3ab*, and *Mbd3abc* KO ESCs (Figure S2B) using CRISPR/Cas9 cleavage and error-prone DNA repair (Cong et al., 2013). We found that *Mbd3c* KO ESCs proliferate similarly to wild-type (WT) cells. In contrast, *Mbd3ab* KO and especially *Mbd3abc* KO ESCs grow more slowly than WT (Figures S2C and S2D), consistent with previous observations of *Mbd3*-null ESCs (Kaji et al., 2006).

Next, we tested the differentiation capacity of each *Mbd3* mutant. Consistent with previous studies (Kaji et al., 2006), we found that ESCs lacking all MBD3 isoforms (*Mbd3abc* KO) maintained expression of both OCT4 and NANOG over 9 days in medium without LIF (Figure 3E). Unlike *Mbd3abc* KOs, *Mbd3c* KOs did not show a noticeable differentiation defect (Figure 3F). ESCs expressing only *Mbd3c* (*Mbd3ab* KO) were largely defective in differentiation (although OCT4 and NANOG levels appeared slightly reduced relative to *Mbd3abc* KO lines). Since *Mbd3c* expression is lost early during differentiation (Figures 3A and 3E), *Mbd3ab* mutants are functionally equivalent to *Mbd3abc* mutants at mid- to late-differentiation time points, potentially accounting for this

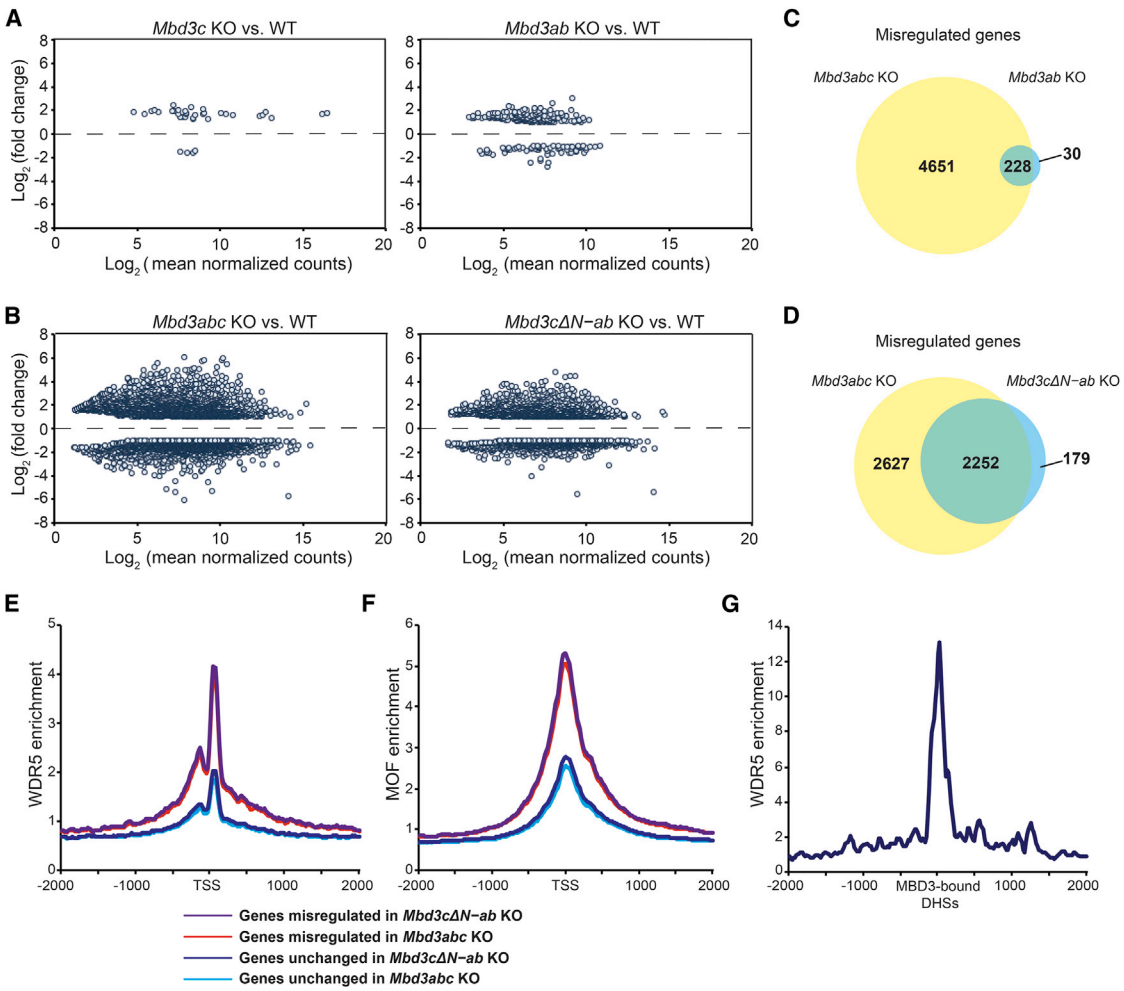

Figure 4. MBD3C Is Redundant with MBD3A and MBD3B in Regulation of Gene Expression

(A and B) MA plots showing $\log_2$ (fold change) in gene expression in *Mbd3c* KO (A, left), *Mbd3ab* KO (A, right), *Mbd3abc* KO (B, left), and *Mbd3cΔN-ab* KO (B, right) ESCs relative to wild-type (WT). Genes shown are misregulated ≥2-fold compared with WT.

(C and D) Venn diagrams showing overlap between misregulated genes in ESCs of indicated genotypes.

(E and F) WDR5 binding (Ang et al., 2011) (E) and MOF binding (Li et al., 2012) (F) averaged over transcription start sites (TSS) of misregulated or unchanged genes in *Mbd3abc* KO (red) and *Mbd3cΔN-ab* KO ESCs (purple).

(G) Average WDR5 binding over MBD3-bound (Yildirim et al., 2011), TSS-distal DNase I hypersensitive sites (DHSs) (GSM1014514).

phenotype. We next asked whether constitutive overexpression of *Mbd3c* in the absence of MBD3A and MBD3B could allow for normal differentiation. To test this possibility, we replaced the entire *Mbd3* gene with an H3F-tagged *Mbd3c* transgene overexpressed from the CAG promoter, which is not silenced during differentiation. Differentiation proceeds normally in these cells (Figure S2E, top panel), revealing that MBD3C can compensate for MBD3A and MBD3B when it is overexpressed. Unexpectedly, ESCs overexpressing *Mbd3cΔN* were also able to differentiate (Figure S2E, bottom panel), in marked contrast to cells expressing *Mbd3cΔN* at endogenous levels (Figure S2F). We conclude that *Mbd3c* is not required for differentiation but can substitute for *Mbd3a* and *Mbd3b* when overexpressed.

MBD3 Isoforms Function Redundantly in Gene Regulation

Although it is dispensable for differentiation, MBD3C binds chromatin (Figure S4) and could still be important for regulation of a subset of MBD3 target genes independently of the other MBD3 isoforms. To test this possibility, we analyzed the transcriptomes of *Mbd3* isoform-specific mutant ESCs by RNA-seq. Gene expression in *Mbd3c* KO ESCs was largely normal (Figure 4A, left panel), with expression of only 38 genes changed more than 2-fold

compared with WT. Similarly, we observed relatively few genes (258) misregulated in *Mbd3ab* KO ESCs that express only *Mbd3c* (Figure 4A, right panel) compared with a much larger number (4,879) misregulated in ESCs where all *Mbd3* isoforms are deleted (Figures 4B [left panel] and 4C). These data suggest that *Mbd3c* can largely compensate for the loss of *Mbd3a* and *Mbd3b* at shared target genes.

To test whether the unique 50-amino-acid MBD3C N terminus (and thus the interaction with WDR5) is important for this compensatory effect, we also performed RNA-seq on ESCs lacking MBD3A and MBD3B and the N terminus of MBD3C (*Mbd3cΔN-ab* KO). In contrast to the relatively few genes misregulated in *Mbd3ab* KO and *Mbd3c* KO cells, we observed 2,431 genes misregulated in *Mbd3cΔN-ab* KO cells, with nearly twice as many genes upregulated as downregulated (1,577 versus 854, respectively; Figure 4B, right panel). The vast majority (~93%) of misregulated genes overlapped with genes misregulated in *Mbd3abc* KO cells (Figure 4D), indicating that the MBD3C N terminus is largely required for MBD3C to compensate for loss of MBD3A and MBD3B. However, as *Mbd3abc* KO has a stronger phenotype than *Mbd3cΔN-ab* KO, MBD3C/NuRD may also regulate some genes independently of its N-terminal domain. Closer examination of the 2,627 genes misregulated only in *Mbd3abc* KO ESCs (Figure 4D) revealed similar, but weaker misregulation in *Mbd3cΔN-ab* KO cells in most cases that fell below our 2-fold cutoff. These data suggest that the *Mbd3cΔN* mutation is not a complete null and are consistent with our finding that MBD3CΔN can compensate for loss of MBD3A and MBD3B during ESC differentiation, but only when overexpressed (Figures S2E and S2F).

WDR5 is a component of multiple complexes with key regulatory functions in ESCs (Ang et al., 2011; Li et al., 2012). *Wdr5* knockdown results in loss of ESC self-renewal (Ang et al., 2011), precluding the use of *Wdr5* KO ESCs to compare the functions of MBD3C and WDR5 in gene regulation. However, to test whether the genes misregulated in *Mbd3c* mutant cells are targets of WDR5 and/or WDR5-associated complexes, we examined published ESC chromatin immunoprecipitation sequencing data for WDR5 and the MSL/NSL subunit MOF (Ang et al., 2011; Li et al., 2012). We observed considerably higher WDR5 binding at the promoter-proximal regions of genes that were misregulated in *Mbd3abc* KO and *Mbd3cΔN-ab* KO cells compared with genes that were unaffected by *Mbd3* mutations (Figure 4E), consistent with a regulatory role for WDR5 at MBD3 target genes. However, it is likely that WDR5 regulates some of these genes through mechanisms independent of MBD3C/NuRD, as we also observed higher MOF binding at genes misregulated in *Mbd3abc* KO and *Mbd3cΔN-ab* KO cells (Figure 4F). Similarly, we found that WDR5 binding is enriched at promoter-distal DNase I hypersensitive sites that are co-bound by MBD3 (Figure 4G), suggesting that WDR5 and MBD3 co-regulate target gene expression at both promoter-distal enhancers and promoters.

We have identified a variant ESC-specific NuRD complex that includes the histone H3 binding protein WDR5. While WDR5 contributes to H3K4 trimethlyation by the SET/MLL complex (Ang et al., 2011; Yang et al., 2014) our data suggest that a WDR5-binding MBD3C/NuRD complex functions separately from SET/MLL. Consistent with these findings, we showed that MBD3C interacts with WDR5 at the same binding surface as MLL1 and histone H3, using a conserved arginine-containing motif (Couture et al., 2006; Patel et al., 2008). As MBD3/NuRD has previously been shown to repress pluripotency genes during differentiation (Reynolds et al., 2012), it is possible that MBD3C/NuRD functions to oppose SET/MLL activity.

Our data reveal an additional layer of complexity to the composition and function of chromatin remodelers in ESCs and uncover a previously unidentified function for the WDR5 protein. The WDR5 binding domain appears to be essential for MBD3C/NuRD function in ESCs, while other MBD3/NuRD complexes are recruited to the same target genes via the MBD or other binding domains. However, since the differentiation defect of *Mbd3ab* KO cells can be overcome by constitutive overexpression of *Mbd3cΔN*, WDR5 may simply enhance the chromatin binding or remodeling activities of MBD3C/NuRD. Multiple independent mechanisms likely target different NuRD complexes to overlapping targets on chromatin, where the complexes function redundantly.

EXPERIMENTAL PROCEDURES

MBD3 Purification and LC-MS/MS

MBD3/NuRD complex was purified from indicated H3F-tagged ESCs as described by Yildirim et al. (2011). Purified samples were separated by SDS-PAGE, and LC-MS/MS was performed as described by Chen et al. (2013).

Embryoid Body Differentiation

ESCs were differentiated to EBs in suspension culture. Cells (2.5×10^6) were plated in ESC medium without LIF in bacteriological plates. Cells were replated to nongelatinized cell culture plates after 3 days and harvested for western blots at the indicated time points.

RNA-Seq

Total RNA was isolated from WT and mutant ESCs using TRIzol (Life Technologies), and purified with the Zymo RNA Clean and Concentrator kit. Strand-specific libraries were prepared and sequenced by Applied Biological Materials, and analyzed as described in Supplemental Experimental Procedures.

ACCESSION NUMBERS

RNA-seq data are available at GEO: GSE80708.

SUPPLEMENTAL INFORMATION

Supplemental Information includes Supplemental Experimental Procedures, four figures, and three tables and can be found with this article online at http://dx.doi.org/10.1016/j.stemcr.2017.04.020.

AUTHOR CONTRIBUTIONS

L.E., K.N.M., and T.G.F. designed and performed most experiments. F.C. designed MS experiments and analyzed data. Y.T. and N.F. performed mass spec experiments. L.E. analyzed RNA-seq data. W.R.H. and M.R.G. designed reprogramming experiments. W.R.H. cloned reprogramming vectors. L.E. and T.G.F. wrote the paper.

ACKNOWLEDGMENTS

We thank Howard Chang for WDR5 binding domain mutant plasmids, Feng Wang and Yong Du for assistance in mouse tissue lysate preparation, and members of the T.G.F. laboratory for critical reading of the manuscript. This research was supported by NIH Grant HD072122 to T.G.F. and NSF Grant CLF1307367 to F.C. T.G.F. is a scholar of the Leukemia and Lymphoma Society. M.R.G. is an Investigator of the Howard Hughes Medical Institute.

Received: April 27, 2016
Revised: April 18, 2017
Accepted: April 20, 2017
Published: May 18, 2017

REFERENCES

Ang, Y.S., Tsai, S.Y., Lee, D.F., Monk, J., Su, J., Ratnakumar, K., Ding, J., Ge, Y., Darr, H., Chang, B., et al. (2011). Wdr5 mediates self-renewal and reprogramming via the embryonic stem cell core transcriptional network. Cell *145*, 183–197.

Bernstein, B.E., Humphrey, E.L., Erlich, R.L., Schneider, R., Bouman, P., Liu, J.S., Kouzarides, T., and Schreiber, S.L. (2002). Methylation of histone H3 Lys 4 in coding regions of active genes. Proc. Natl. Acad. Sci. USA *99*, 8695–8700.

Bode, D., Yu, L., Tate, P., Pardo, M., and Choudhary, J. (2016). Characterization of two distinct nucleosome remodeling and deacetylase (NuRD) complex assemblies in embryonic stem cells. Mol. Cell. Proteomics *15*, 878–891.

Chen, P.B., Hung, J.H., Hickman, T.L., Coles, A.H., Carey, J.F., Weng, Z., Chu, F., and Fazzio, T.G. (2013). Hdac6 regulates Tip60-p400 function in stem cells. Elife *2*, e01557. http://dx.doi.org/10.7554/eLife.01557.

Cong, L., Ran, F.A., Cox, D., Lin, S., Barretto, R., Habib, N., Hsu, P.D., Wu, X., Jiang, W., Marraffini, L.A., et al. (2013). Multiplex genome engineering using CRISPR/Cas systems. Science *339*, 819–823.

Couture, J.F., Collazo, E., and Trievel, R.C. (2006). Molecular recognition of histone H3 by the WD40 protein WDR5. Nat. Struct. Mol. Biol. *13*, 698–703.

Denslow, S.A., and Wade, P.A. (2007). The human Mi-2/NuRD complex and gene regulation. Oncogene *26*, 5433–5438.

Dias, J., Van Nguyen, N., Georgiev, P., Gaub, A., Brettschneider, J., Cusack, S., Kadlec, J., and Akhtar, A. (2014). Structural analysis of the KANSL1/WDR5/KANSL2 complex reveals that WDR5 is required for efficient assembly and chromatin targeting of the NSL complex. Genes Dev. *28*, 929–942.

dos Santos, R.L., Tosti, L., Radzisheuskaya, A., Caballero, I.M., Kaji, K., Hendrich, B., and Silva, J.C.R. (2014). MBD3/NuRD facilitates induction of pluripotency in a context-dependent manner. Cell Stem Cell *15*, 102–110.

Dou, Y., Milne, T.A., Ruthenburg, A.J., Lee, S., Lee, J.W., Verdine, G.L., Allis, C.D., and Roeder, R.G. (2006). Regulation of MLL1 H3K4 methyltransferase activity by its core components. Nat. Struct. Mol. Biol. *13*, 713–719.

Han, Z., Guo, L., Wang, H., Shen, Y., Deng, X.W., and Chai, J. (2006). Structural basis for the specific recognition of methylated histone H3 lysine 4 by the WD-40 protein WDR5. Mol. Cell *22*, 137–144.

Hendrich, B., and Bird, A. (1998). Identification and characterization of a family of mammalian methyl-CpG binding proteins. Mol. Cell. Biol. *18*, 6538–6547.

Hendrich, B., Guy, J., Ramsahoye, B., Wilson, V.A., and Bird, A. (2001). Closely related proteins MBD2 and MBD3 play distinctive but interacting roles in mouse development. Genes Dev. *15*, 710–723.

Hotta, A., Cheung, A.Y.L., Farra, N., Vijayaragavan, K., Séguin, C.A., Draper, J.S., Pasceri, P., Maksakova, I.A., Mager, D.L., Rossant, J., et al. (2009). Isolation of human iPS cells using EOS lentiviral vectors to select for pluripotency. Nat. Methods *6*, 370–376.

Kaji, K., Caballero, I.M., MacLeod, R., Nichols, J., Wilson, V.A., and Hendrich, B. (2006). The NuRD component Mbd3 is required for pluripotency of embryonic stem cells. Nat. Cell Biol. *8*, 285–292.

Kim, J., Chu, J., Shen, X., Wang, J., and Orkin, S.H. (2008). An extended transcriptional network for pluripotency of embryonic stem cells. Cell *132*, 1049–1061.

Li, X., Li, L., Pandey, R., Byun, J.S., Gardner, K., Qin, Z., and Dou, Y. (2012). The histone acetyltransferase MOF is a key regulator of the embryonic stem cell core transcriptional network. Cell Stem Cell *11*, 163–178.

Odho, Z., Southall, S.M., and Wilson, J.R. (2010). Characterization of a novel WDR5-binding site that recruits RbBP5 through a conserved motif to enhance methylation of histone H3 lysine 4 by mixed lineage leukemia protein-1. J. Biol. Chem. *285*, 32967–32976.

Patel, A., Vought, V.E., Dharmarajan, V., and Cosgrove, M.S. (2008). A conserved arginine-containing motif crucial for the assembly and enzymatic activity of the mixed lineage leukemia protein-1 core complex. J. Biol. Chem. *283*, 32162–32175.

Reynolds, N., Salmon-Divon, M., Dvinge, H., Hynes-Allen, A., Balasooriya, G., Leaford, D., Behrens, A., Bertone, P., and Hendrich, B. (2011). NuRD-mediated deacetylation of H3K27 facilitates recruitment of Polycomb Repressive Complex 2 to direct gene repression. EMBO J. *31*, 593–605.

Reynolds, N., Latos, P., Hynes-Allen, A., Loos, R., Leaford, D., O'Shaughnessy, A., Mosaku, O., Signolet, J., Brennecke, P., Kalkan, T., et al. (2012). NuRD suppresses pluripotency gene expression to promote transcriptional heterogeneity and lineage commitment. Cell Stem Cell *10*, 583–594.

Ruthenburg, A.J., Wang, W., Graybosch, D.M., Li, H., Allis, C.D., Patel, D.J., and Verdine, G.L. (2006). Histone H3 recognition and presentation by the WDR5 module of the MLL1 complex. Nat. Struct. Mol. Biol. *13*, 704–712.

Saito, M., and Ishikawa, F. (2002). The mCpG-binding domain of human MBD3 does not bind to mCpG but interacts with NuRD/Mi2 components HDAC1 and MTA2. J. Biol. Chem. *277*, 35434–35439.

Santos-Rosa, H., Schneider, R., Bannister, A.J., Sherriff, J., Bernstein, B.E., Emre, N.C.T., Schreiber, S.L., Mellor, J., and Kouzarides, T. (2002). Active genes are tri-methylated at K4 of histone H3. Nature *419*, 407–411.

Schuetz, A., Allali-Hassani, A., Martín, F., Loppnau, P., Vedadi, M., Bochkarev, A., Plotnikov, A.N., Arrowsmith, C.H., and Min, J. (2006). Structural basis for molecular recognition and presentation of histone H3 by WDR5. EMBO J. *25*, 4245–4252.

Song, J.J., and Kingston, R.E. (2008). WDR5 interacts with mixed lineage leukemia (MLL) protein via the histone H3-binding pocket. J. Biol. Chem. *283*, 35258–35264.

Tong, J.K., Hassig, C.A., Schnitzler, G.R., Kingston, R.E., and Schreiber, S.L. (1998). Chromatin deacetylation by an ATP-dependent nucleosome remodelling complex. Nature *395*, 917–921.

Wade, P.A., Jones, P.L., Vermaak, D., and Wolffe, A.P. (1998). A multiple subunit Mi-2 histone deacetylase from Xenopus laevis cofractionates with an associated Snf2 superfamily ATPase. Curr. Biol. *8*, 843–846.

Wysocka, J., Swigut, T., Milne, T.A., Dou, Y., Zhang, X., Burlingame, A.L., Roeder, R.G., Brivanlou, A.H., and Allis, C.D. (2005). WDR5 associates with histone H3 methylated at K4 and is essential for H3 K4 methylation and vertebrate development. Cell *121*, 859–872.

Xue, Y., Wong, J., Moreno, G.T., Young, M.K., Côté, J., and Wang, W. (1998). NURD, a novel complex with both ATP-dependent chromatin-remodeling and histone deacetylase activities. Mol. Cell *2*, 851–861.

Yang, Y.W., Flynn, R.A., Chen, Y., Qu, K., Wan, B., Wang, K.C., Lei, M., and Chang, H.Y. (2014). Essential role of lncRNA binding for WDR5 maintenance of active chromatin and embryonic stem cell pluripotency. Elife *3*, e02046.

Yildirim, O., Li, R., Hung, J.H., Chen, P.B., Dong, X., Ee, L.S., Weng, Z., Rando, O.J., and Fazzio, T.G. (2011). Mbd3/NURD complex regulates expression of 5-hydroxymethylcytosine marked genes in embryonic stem cells. Cell *147*, 1498–1510.

Zhang, Y., LeRoy, G., Seelig, H.P., Lane, W.S., and Reinberg, D. (1998). The dermatomyositis-specific autoantigen Mi2 is a component of a complex containing histone deacetylase and nucleosome remodeling activities. Cell *95*, 279–289.

Zhang, Y., Ng, H.H., Erdjument-Bromage, H., Tempst, P., Bird, A., and Reinberg, D. (1999). Analysis of the NuRD subunits reveals a histone deacetylase core complex and a connection with DNA methylation. Genes Dev. *13*, 1924–1935.

Stem Cell Reports, Volume *8*

Supplemental Information

An Embryonic Stem Cell-Specific NuRD Complex Functions through Interaction with WDR5

Ly-Sha Ee, Kurtis N. McCannell, Yang Tang, Nancy Fernandes, W. Rod Hardy, Michael R. Green, Feixia Chu, and Thomas G. Fazzio

SUPPLEMENTAL INFORMATION

SUPPLEMENTAL FIGURES

Figure S1. MBD3C contains a unique 50-amino acid N-terminus and forms an ESC-specific NuRD complex, related to Figure 1. (A) Left: Schematic of the three MBD3 isoforms in ESCs. MBD3A contains a methyl-binding domain (MBD) that is truncated in MBD3b and absent in MBD3C. The purple box signifies the unique MBD3 N-terminal 50 amino acids. Right: Western blot of MBD3 in ESCs and MEFs. Actin serves as a loading control. **(B)** Western blots of NuRD subunits from purified H3F-WDR5 complexes in WT, *Mbd3c* KO or *Mbd3abc* KO ESCs. **(C)** Schematic of the N-terminal *Mbd3c* DNA and MBD3C protein sequences determined by 5'RACE. Exons are indicated by numbered blue boxes, introns by connecting black lines. The sequence of *Mbd3* intron 2 is shown, with the *Mbd3c* N-terminus in red. The amino acid sequence of the MBD3C N-terminus derived from intron 2 is shown (represented by the gray box in the *Mbd3c* gene). **(D)** Table of peptide counts from mass spec analysis of individually FLAG-tagged MBD3 isoforms. **(E)** Glycerol gradient analysis of *Mbd3-H3F* nuclear extracts.

Figure S2. Characterization of MBD3 isoform KO ESC lines, related to Figure 3. (A) Western blot of MBD3 from lysates of the indicated mouse tissues. Actin blot and Coomassie stain are shown as loading controls. **(B)** Western blot of MBD3 expression in MBD3 isoform KO ESCs generated through CRISPR/Cas9. **(C-D)** Growth curves for *Mbd3c* KO **(C)** and *Mbd3ab* and *Mbd3abc* KO **(D)** ESC lines, relative to wildtype (WT) ESCs. Error bars represent +/- standard deviation of three replicate experiments performed on each clonal replicate. **(E)** Western blots of indicated proteins during differentiation of WT, *Mbd3abc* KO ESCs overexpressing *Mbd3c-H3F*, or *Mbd3abc* KO ESCs overexpressing *Mbd3cΔN-H3F.* **(F)** Western blots of indicated proteins during differentiation of WT or *Mbd3cΔN–ab* KO ESCs.

Figure S3. Images of dox-induced reprogrammed colonies, related to Figure 3. (A) Representative images of EOS-EGFP positive/OSK-mCherry negative iPSCs at reprogramming Day 30, 10 days after dox removal (left) and an iPSC line derived from a single colony (right). Scale bars = 400μm. **(B)** Representative AP staining of iPSCs at reprogramming Day 31.

Figure S4. Chromatin extraction assay, related to Figure 4. (A) Western blot of MBD3 from salt fractionation of chromatin from WT ESC nuclei. Protein released at indicated concentrations of NaCl is shown. RNA Pol II is included as a control.

SUPPLEMENTAL EXPERIMENTAL PROCEDURES

Cell Culture and Generation of ESC lines

Murine ESCs are derived from E14 and cultured on gelatin-coated plates as previously described (Chen et al., 2013). *Mbd3a-H3F*, *Mbd3c-H3F*, and *Mbd3cΔN-H3F* ESCs were generated by infection of E14 with pLJM1 lentiviral vectors carrying the respective constructs.

The H3F-WDR5 targeting construct was made by inserting PCR-produced homology arms (959 and 561 bp) and an H3F tag into pBluescript II SK+ (Stratagene). Oligos were inserted into pX330-puro^R to target to the N-terminus of WDR5. The plasmids were transfected with FuGENE HD (Promega) into E14, *Mbd3c* KO, and *Mbd3abc* KO cells. Clones were selected with puromycin and screened by PCR, sequencing, and western blot.

Expression of MBD3C and WDR5 domain mapping mutants

MBD3C-H3F, V5-WDR5 constructs and the indicated WDR5 mutants (Yang et al., 2014) were cloned into pCAGGS-IRES-Hygro^R using the 5' XhoI site and the 3' EcoRI site. pCAGGS-V5-WDR5 was created from a synthesized full-length mouse *Wdr5*. MBD3A-H3F and truncations of MBD3C-H3F with XhoI and MfeI restriction sites were derived by PCR on *Mbd3*-H3F sequences and cloned into the vector. The MBD3C Δ41-50 and R43A mutant constructs were made by PCR on pCAGGS-MBD3C-H3F with primers incorporating the mutations and flanking primers and then digesting the new sequences and ligating them into the vector. pCAGGS–cN41-50–MBD3A-H3F was made by synthesizing the N-terminus and inserting it into the MBD3A plasmid using the XhoI site and a gene-internal BamHI site. Plasmids were transiently transfected into 293T cells using FuGENE HD (Promega), and the cells were harvested for IP after 2 days.

Generation of MBD3 isoform KO ESCs

Mbd3ab, *Mbd3c*, *Mbd3abc*, and *Mbd3cΔN-ab* KO ESC lines were generated using the CRISPR/Cas9 system (Cong et al., 2013) to introduce mutations into *Mbd3* exon 2 (*Mbd3ab* KO and *Mbd3cΔN−ab* KO), intron 2 (*Mbd3c* KO), or exon 5 (*Mbd3abc* KO). Guide RNAs targeting *Mbd3ab*, *Mbd3c*, or *Mbd3abc* (see Table S3 for sequences) were cloned into the pX330-puro^R vector and transfected into E14 ESCs as described (Hainer et al., 2015). Individual clones were screened by TOPO cloning (Invitrogen) and sequencing to verify the presence of homozygous frameshift mutations. ESC lines were further screened by western blot to verify loss of the appropriate MBD3 isoform(s). To create the *Mbd3cΔN−ab* KO line, we first transfected the pX330 plasmid targeting *Mbd3c* into E14 ESCs along with a donor plasmid containing the *Mbd3c* coding sequence with a 50-amino acid N-terminal deletion. The donor plasmid was generated by annealing oligos to make the *Mbd3cΔN* cDNA construct and cloning along with ~2kb homology arms flanking the *Mbd3c* start site into pBluescript SK II+ (Stratagene). Verified *Mbd3cΔN* ESC lines were then retargeted using the *Mbd3ab* KO guide RNA plasmid and screened as described above.

Mbd3abc KO/Mbd3c o/e ESC lines were made by replacing the endogenous *Mbd3* locus with a construct containing PCR-produced homology arms (2070 and 1649 bp), the full CAGGS promoter, and a modified *Mbd3c*-H3F-polyA sequence without CpGs in the gene or tag. The *Mbd3abc* KO – cΔN o/e construct was made using PCR and restriction digestion to delete the 150 bp corresponding to the unique N-terminus of MBD3C. Oligos were inserted into two CRISPR plasmids (pX330-puro^R) and transfected into E14 cells as described above. Clones were selected with puromycin and screened by PCR, sequencing, and western blot.

5'RACE
5'RACE was performed on 4µg total RNA using the 5'RACE System Version 2.0 kit (Invitrogen). See Table S3 for primer sequences.

MBD3 Purification, WDR5 Purification, and LC-MS/MS
MBD3/NuRD complex was purified from MBD3-H3F, MBD3A-H3F, MBD3C-H3F, and MBD3CΔN-H3F ESCs as described (Yildirim et al., 2011). Purified samples were separated by SDS-PAGE, stained with SimplyBlue SafeStain (Invitrogen), and LC-MS/MS was performed as described in (Chen et al., 2013). For WDR5 complex purification, nuclear fractions were isolated from H3F-WDR5 ESCs using the NE-PER kit (Thermo), diluted 1:3 in MVL buffer (50mM Tris, pH 7.5; 250mM NaCl; 0.1% Triton X-100), and purified similarly, omitting the His purification step.

Western Blotting and Immunoprecipitation
Western blots were performed with the following antibodies: anti-MBD3 (Bethyl A302-528A and Abgent AM2203B), anti-FLAG (M2, Sigma F1804), anti-WDR5 (Bethyl A302-429A and A302-430A), anti-OCT4 (Santa Cruz sc-8628), anti-NANOG (Bethyl A300-398A), anti-MTA1 (Bethyl A300-911A), anti-MTA2 (Santa Cruz sc-28731), anti-CHD4 (Bethyl A301-082A) anti–β-ACTIN (Sigma A1978), anti–RNA POLYMERASE II (Santa Cruz sc-899), anti-RBBP4 (Bethyl A301-206A), anti-RBBP7 (Bethyl A300-958A), anti-LSD1 (Bethyl A300-215A), anti-p66α (Bethyl A302-358A), anti-p66β (Bethyl A301-281A), anti-HDAC1 (Bethyl A300-713A), anti-HDAC2 (Bethyl A300-705A), anti-ASH2L (Bethyl A300-112A), anti-V5 (Invitrogen 46-0705). Mouse tissue lysates were prepared by homogenizing indicated tissues in lysis buffer (50mM Tris-HCl pH 7.5; 150mM NaCl; 0.5% Triton X-100; 5% glycerol; 1mM PMSF). For IP, nuclear lysates were prepared using the NE-PER kit (Thermo). FLAG IP was performed as described in (Chen et al., 2013). MBD3 IPs in ESCs and 293T cells were performed similarly, except washes were performed in MVL buffer + 1mM EDTA.

Glycerol Gradient Analysis
Nuclear extracts were prepared from *Mbd3-H3F* ESCs using the NE-PER kit (Thermo). Nuclear extract (1470µg) was diluted in MVL buffer and spun in a 10-40% glycerol gradient at 37krpm for 17 hours in a Beckmann L-90K ultracentrifuge. 29 fractions were collected and odd fractions western blotted with the indicated antibodies.

Embryoid Body Differentiation
ESCs were differentiated to embryoid bodies (EBs) in suspension culture. 2.5 x 10^6 cells were plated in ESC medium without LIF in bacteriological plates. Cells were replated to non-gelatinized cell culture plates after 3 days and harvested for western blots at the indicated timepoints.

Chromatin Extraction Assay
Chromatin was extracted from WT ESCs by salt fractionation as described (Henikoff et al., 2009). Briefly, 4 x 10^7 cells were pelleted, washed in PBS, and resuspended in TM2 buffer (10mM Tris-HCl pH 7.5, 2mM $MgCl_2$, 1.5% NP-40, 1x HALT protease inhibitor

cocktail) on ice for 5min. Cells were pelleted and the nuclei incubated in TM2 + 70mM NaCl for 2h at 4°C. Nuclei were pelleted and incubated as before in TM2 + 140mM NaCl, and further pelleted and incubated in TM2 + 600mM NaCl overnight at 4°C. Supernatants from each incubation were saved as 0, 70,140 and 600mM NaCl fractions, clarified by centrifugation at full speed, and western blotted with the indicated antibodies.

Reprogramming to pluripotent stem cells

Lentiviral plasmids for dox-inducible Oct4, Sox2, and Klf4 expression (pLenti-Tet-OSK-mCherry) and for L-Myc expression (pLenti-Tet-L-Myc) were generated by digestion of CMV-OSK and CMV-L-Myc cDNA from FUW-OSKM and pMXs-Ms-L-Myc (Addgene 20328 and 26023 respectively) and cloning into pcDNA3.1 with HIV1-based 5' and 3' LTRs from pGIPZ. To package lentivirus, 293T cells were transfected with 5µg pLenti-Tet-OSK-mCherry, pLenti-Tet-L-Myc, FUW-rTtA (Addgene 20342), or EOS-EGFP (Addgene 21313) lentiviral reporter plasmids along with packaging plasmids (5µg psPAX2 and 2.5µg pCMV-VSV-G (Addgene)). Primary MEFs were infected with day 2 viral supernatant using 8µg/mL hexadimethrine bromide (Sigma), and re-infected after 24 hours. MEFs were replated in ESC media after 48 hours and induced with 2µg/ml dox 4 days after the first infection. Dox was removed at day 20 and cells were cultured for an additional 10 days. On Day 30 cells were imaged to assess loss of OSK transgenes and EOS-EGFP reporter activation, and on day 31 were stained for alkaline phosphatase according to kit instructions (Millipore). Single colonies were picked on Day 30, expanded, and western blotted with the indicated antibodies. Media were changed every other day.

Bisulfite pyrosequencing

WT ESCs were subjected to embryoid body differentiation and harvested at the indicated timepoints. Briefly, genomic DNA was phenol-chloroform extracted from cells incubated in ES cell lysis buffer (10 mM Tris, pH 7.5; 10 mM EDTA; 10 mM NaCl; 0.5% sarkosyl) with 1 µg/µL proteinase K at 55°C overnight. The DNA was bisulfite converted using the EpiTect Bisulfite Kit (QIAGEN). Primers were designed for the *Mbd3c* CpG island using PyroMark Q24 software (QIAGEN, see Table S3 for sequences), with one PCR primer in a pair biotinylated, and PCR was performed on the converted DNA with KAPA HiFi HotStart Uracil+ ReadyMix (Kapa Biosystems). PCR products were bound to streptavidin sepharose beads (GE Healthcare) and sequenced using a PyroMark Q24 (QIAGEN). Data were analyzed using PyroMark Q24 software.

RNA-seq

Total RNA was isolated from two biological replicate WT, *Mbd3ab* KO, *Mbd3c* KO, *Mbd3abc* KO, and *Mbd3cΔN−ab* KO ESC lines using TRIzol (Life Technologies), and purified with the Zymo RNA Clean and Concentrator kit. 2µg RNA was used for library preparation. RNA was rRNA-depleted (NEB and Clontech) and strand-specific libraries were prepared using the TruSeq Stranded mRNA LT kit (Illumina).

RNA-seq data analysis

Reads were mapped to the mouse mm10 genome with TopHat2 (Kim et al., 2013), using parameters --library-type fr-firststrand --segment-length 38. Mapped reads were processed in HOMER (Heinz et al., 2010) using the “analyzeRepeats” command to calculate raw counts and normalized reads per kilobase per million mapped reads (rpkm) for each gene. Differential gene expression was calculated with DESeq2 (Love et al., 2014) using the “getDiffExpression” command in HOMER. Genes with an adjusted p value < 0.05 and log2 (fold change) were considered significantly changed.

To map WDR5 and Mof binding at TSSs of significantly changed genes, WDR5 (Ang et al., 2011) and Mof (Li et al., 2012) ChIP-seq data were downloaded from GEO (GSE22934 and GSE37268) and aligned to the mouse mm10 genome using Bowtie (Langmead et al., 2009). Mapped reads were processed in HOMER using the “annotatePeaks” command. For Mof ChIP-seq, 2 replicate libraries were averaged in the aggregation plot.

To map WDR5 at MBD3-bound DNase I hypersensitive sites (DHSs), peaks were called from MBD3 ChIP-seq data (Yildirim et al., 2011; GSE31690) using the HOMER “findPeaks” command, and MBD3-bound DHSs were identified using the “mergePeaks” command with peaks called from mouse ENCODE DHSs (GSM1014154) without TSSs. The WDR5 ChIP-seq library was aligned to the MBD3-bound DHS peak data using the “annotatePeaks” command.

SUPPLEMENTAL TABLES

Table S1, related to Figure 1. Proteins identified in LC-MS/MS of endogenous MBD3-H3F ESCs.

Table S2, related to Figure 1. Proteins identified in LC-MS/MS of pLJM1- MBD3A-H3F, MBD3C-H3F, and MBD3CΔN-H3F ESCs.

Table S3, related to Supplemental Experimental Procedures. Oligonucleotides used in this study.

SUPPLEMENTAL REFERENCES

Ang, Y.-S., Tsai, S.-Y., Lee, D.-F., Monk, J., Su, J., Ratnakumar, K., Ding, J., Ge, Y., Darr, H., Chang, B., et al. (2011). Wdr5 Mediates Self-Renewaland Reprogramming via the Embryonic Stem Cell Core Transcriptional Network. Cell *145*, 183–197.

Chen, P.B., Hung, J.-H., Hickman, T.L., Coles, A.H., Carey, J.F., Weng, Z., Chu, F., and Fazzio, T.G. (2013). Hdac6 regulates Tip60-p400 function in stem cells. eLife *2*, e01557.

Cong, L., Ran, F.A., Cox, D., Lin, S., Barretto, R., Habib, N., Hsu, P.D., Wu, X., Jiang, W., Marraffini, L.A., et al. (2013). Multiplex genome engineering using CRISPR/Cas systems. Science *339*, 819–823.

Hainer, S.J., Gu, W., Carone, B.R., Landry, B.D., Rando, O.J., Mello, C.C., and Fazzio,

T.G. (2015). Suppression of pervasive noncoding transcription in embryonic stem cells by esBAF. Genes Dev. *29*, 362–378.

Heinz, S., Benner, C., Spann, N., Bertolino, E., Lin, Y.C., Laslo, P., Cheng, J.X., Murre, C., Singh, H., and Glass, C.K. (2010). Simple combinations of lineage-determining transcription factors prime cis-regulatory elements required for macrophage and B cell identities. Mol. Cell *38*, 576–589.

Henikoff, S., Henikoff, J.G., Sakai, A., Loeb, G.B., and Ahmad, K. (2009). Genome-wide profiling of salt fractions maps physical properties of chromatin. Genome Res. *19*, 460–469.

Kim, D., Pertea, G., Trapnell, C., Pimentel, H., Kelley, R., and Salzberg, S.L. (2013). TopHat2: accurate alignment of transcriptomes in the presence of insertions, deletions and gene fusions. Genome Biol. *14*, R36.

Langmead, B., Trapnell, C., Pop, M., and Salzberg, S.L. (2009). Ultrafast and memory-efficient alignment of short DNA sequences to the human genome. Genome Biol. *10*, R25.

Li, X., Li, L., Pandey, R., Byun, J.S., Gardner, K., Qin, Z., and Dou, Y. (2012). The histone acetyltransferase MOF is a key regulator of the embryonic stem cell core transcriptional network. Cell Stem Cell *11*, 163–178.

Love, M.I., Huber, W., and Anders, S. (2014). Moderated estimation of fold change and dispersion for RNA-seq data with DESeq2. Genome Biol. *15*, 550.

Yang, Y.W., Flynn, R.A., Chen, Y., Qu, K., Wan, B., Wang, K.C., Lei, M., and Chang, H.Y. (2014). Essential role of lncRNA binding for WDR5 maintenance of active chromatin and embryonic stem cell pluripotency. eLife *3*, e02046.

Yildirim, O., Li, R., Hung, J.-H., Chen, P.B., Dong, X., Ee, L.-S., Weng, Z., Rando, O.J., and Fazzio, T.G. (2011). Mbd3/NURD Complex Regulates Expression of 5-Hydroxymethylcytosine Marked Genes in Embryonic Stem Cells. Cell *147*, 1498–1510.

Figure S1

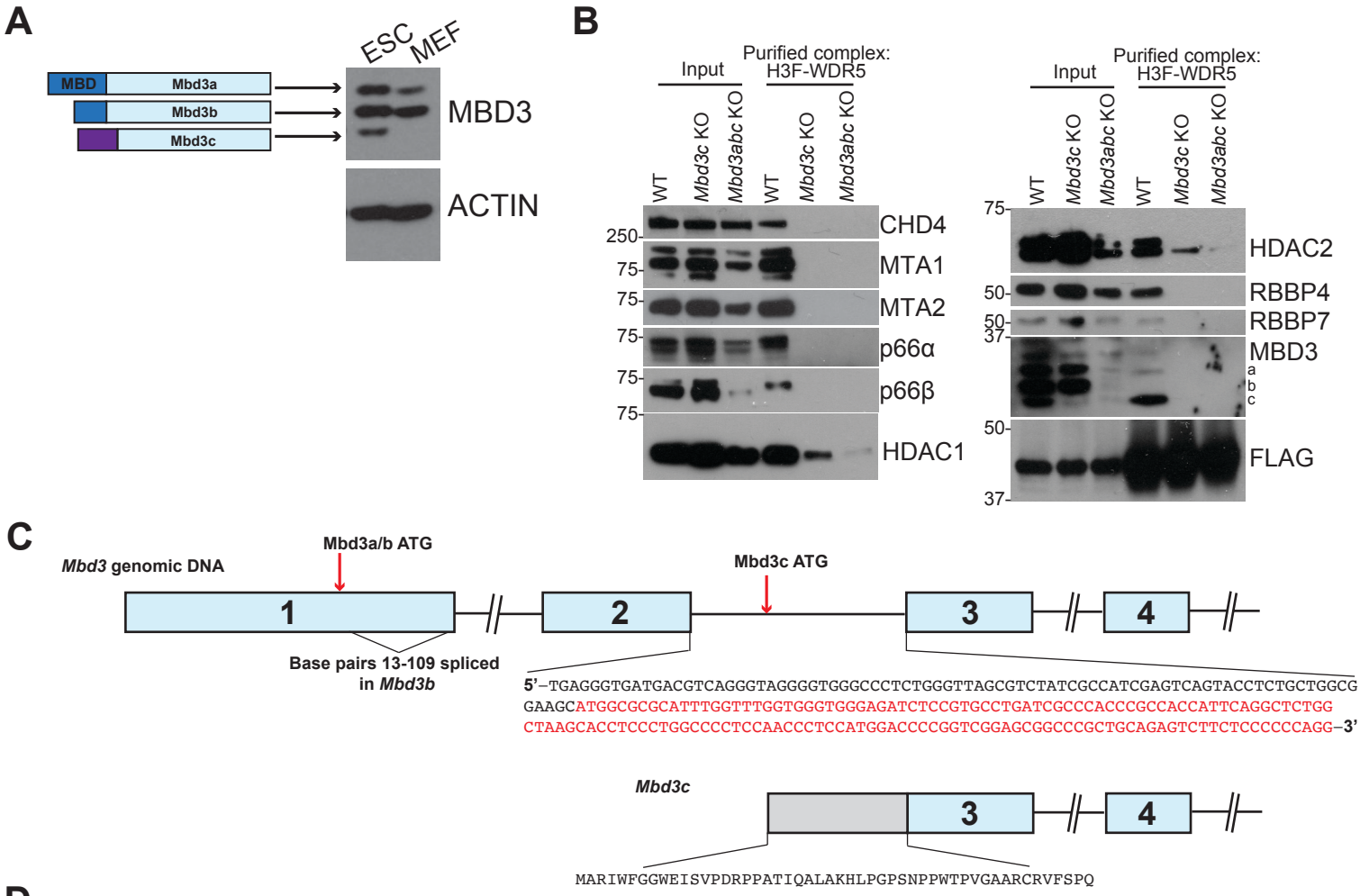

D

Peptide count			NuRD complex protein
MBD3A-H3F	MBD3C-H3F	MBD3CΔN-H3F	
322	291	365	Chromodomain-helicase-DNA-binding protein 4
396	503	493	Metastasis-associated protein MTA2
382	203	425	Metastasis-associated protein MTA1
381	375	445	Metastasis-associated protein MTA3
428	527	674	Transcriptional repressor p66-alpha
343	414	543	Transcriptional repressor p66-beta
268	271	308	Histone deacetylase 1
193	183	213	Histone deacetylase 2
213	208	320	Methyl-CpG-binding domain protein 3
200	250	280	Histone-binding protein RBBP4
163	157	180	Histone-binding protein RBBP7
2	157	3	WD repeat-containing protein 5

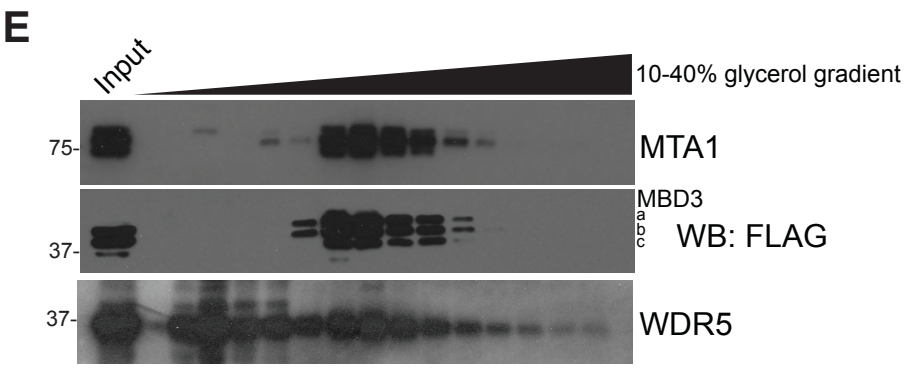

Figure S2

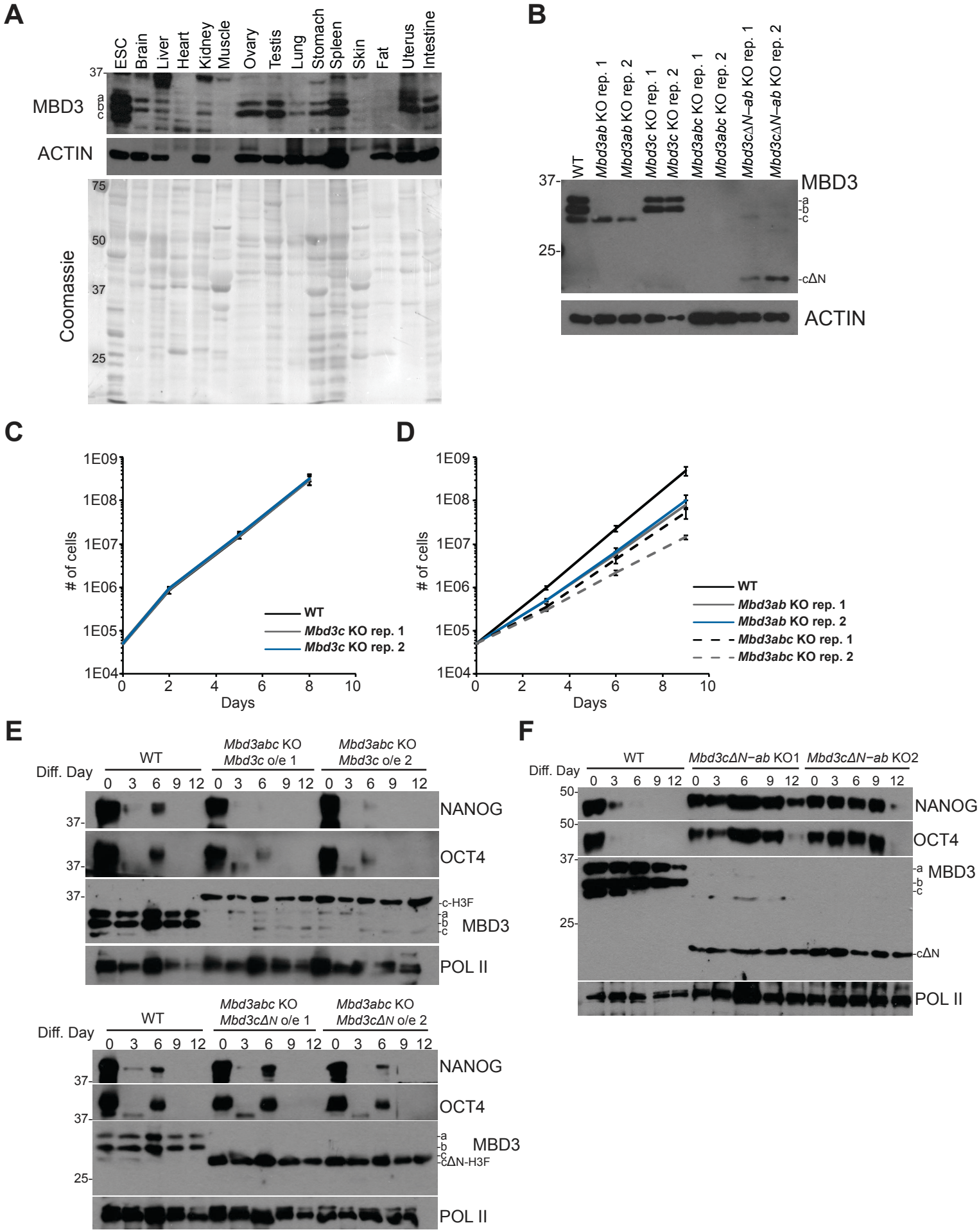
A
ESC
Brain
Liver
Heart
Kidney
Muscle
Ovary
Testis
Lung
Stomach
Spleen
Skin
Fat
Uterus
Intestine
37
MBD3
a
b
c
ACTIN
75
50
37
25
Coomassie
B
WT
Mbd3ab KO rep. 1
Mbd3ab KO rep. 2
Mbd3c KO rep. 1
Mbd3c KO rep. 2
Mbd3abc KO rep. 1
Mbd3abc KO rep. 2
Mbd3cΔN–ab KO rep. 1
Mbd3cΔN–ab KO rep. 2
37
25
MBD3
a
b
c
cΔN
ACTIN
C
1E09
1E08
1E07
1E06
1E05
1E04
# of cells
0
2
4
6
8
10
Days
WT
Mbd3c KO rep. 1
Mbd3c KO rep. 2
D
1E09
1E08
1E07
1E06
1E05
1E04
# of cells
0
2
4
6
8
10
Days
WT
Mbd3ab KO rep. 1
Mbd3ab KO rep. 2
Mbd3abc KO rep. 1
Mbd3abc KO rep. 2
E
Diff. Day
WT
Mbd3abc KO Mbd3c o/e 1
Mbd3abc KO Mbd3c o/e 2
0 3 6 9 12 0 3 6 9 12 0 3 6 9 12
37
NANOG
37
OCT4
37
c-H3F
a
b
c
MBD3
POL II
Diff. Day
WT
Mbd3abc KO Mbd3cΔN o/e 1
Mbd3abc KO Mbd3cΔN o/e 2
0 3 6 9 12 0 3 6 9 12 0 3 6 9 12
37
NANOG
37
OCT4
37
25
a
b
c
MBD3
cΔN-H3F
POL II
F
Diff. Day
WT
Mbd3cΔN–ab KO1
Mbd3cΔN–ab KO2
0 3 6 9 12 0 3 6 9 12 0 3 6 9 12
50
NANOG
50
OCT4
37
25
a
b
c
MBD3
cΔN
POL II

Figure S3

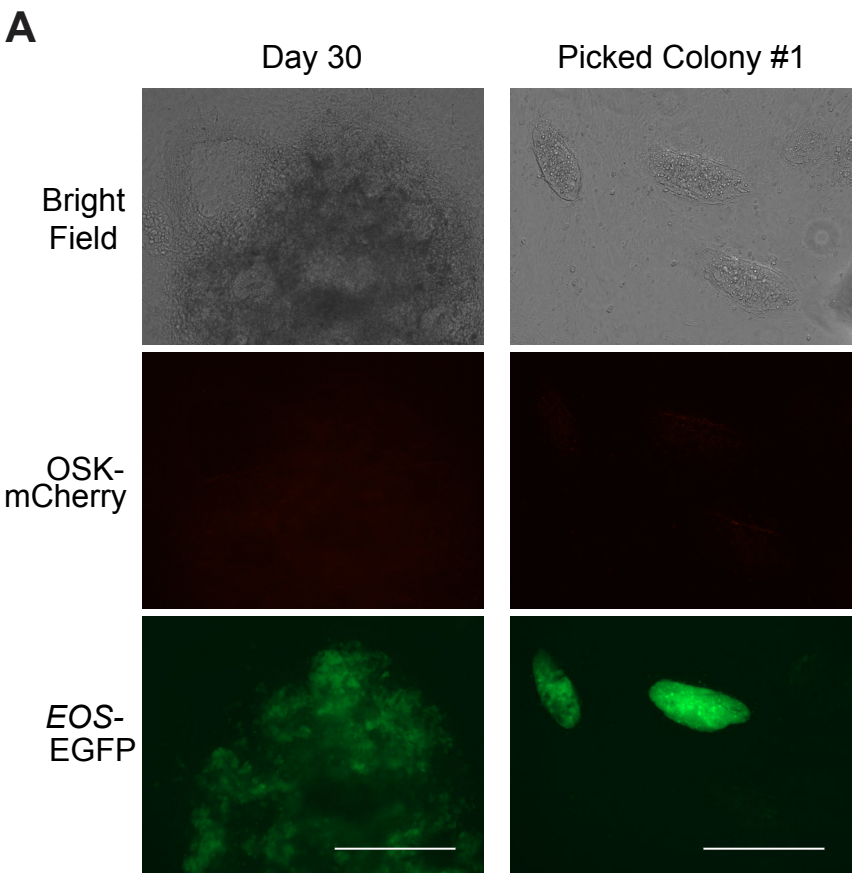
A
Day 30
Picked Colony #1
Bright Field
OSK-mCherry
EOS-EGFP
B
Day 31
Alkaline phosphatase

Figure S4